Level-crossing resonances on open atomic transitions in a buffered Cs vapor cell: Linewidth narrowing, high contrast, and atomic magnetometry applications

D. V. Brazhnikov [1,2,*], V. I. Vishnyakov,[1] A. N. Goncharov [1,2,3] E. Alipieva [4]
C. Andreeva [4,5] and E. Taskova [4]

[1]*Institute of Laser Physics, SB RAS, 15B Lavrentyev Avenue, Novosibirsk 630090, Russia*
[2]*Quantum Electronics Department, Novosibirsk State University, 1 Pirogov Street, Novosibirsk 630090, Russia*
[3]*Laser Systems Department, Novosibirsk State Technical University, 20 Karl Marks Avenue, Novosibirsk 630073, Russia*
[4]*Institute of Electronics, Bulgarian Academy of Sciences, 72 Tsarigradsko Chaussee, Sofia 1784, Bulgaria*
[5]*Faculty of Physics, Sofia University "St. Kliment Ohridski," 5 James Bourchier Boulevard, Sofia 1164, Bulgaria*

The ground-state Hanle effect (GSHE) in alkali-metal atomic vapor using a single circularly polarized light wave underlies one of the most reliable and simple techniques of modern atomic magnetometry. This effect causes a narrow (subnatural-width) resonance in the light wave intensity passing through the vapor cell. The GSHE-based sensors typically operate in the so-called spin-exchange relaxation-free (SERF) regime to reduce the resonance linewidth. However, this regime requires a relatively high temperature of vapors (approximately equal to 150 °C), leading to high heat release and power consumption of the sensor head. In addition, without applying special measures, the SERF regime significantly limits the dynamic range of measurements. Here we study a pump-probe scheme involving a single elliptically polarized light wave and a polarimetric detection technique. The wave is in resonance with two adjacent optical transitions in the cesium D_1 line ($\lambda \approx 894.5$ nm) due to their overlap in the presence of a buffer gas (130 Torr neon). Using a small ($V \approx 0.1$ cm^3) glass vapor cell, we demonstrate the possibility to observe subnatural-width resonances with a high contrast-to-width ratio (up to 45%/mG) in low-temperature (60 °C) operation due to strong light-induced circular dichroism in the medium. Based on the Λ scheme of atomic energy levels, we obtain explicit analytical expressions for the shape of the resonance line. The model reveals a linewidth narrowing effect due to openness of the level scheme. The observed bright features are unusual for magneto-optical atomic spectroscopy as openness is commonly considered to be an undesirable effect that degrades resonance characteristics. Measuring the noise voltage, we estimate the sensitivity of the magnetic-field measurements to be 1.8 pT/$\sqrt{\text{Hz}}$ with a sensitivity of 60 fT/$\sqrt{\text{Hz}}$ in the photon-shot-noise limit. In general, the results contribute to the theory of GSHE resonances and also can be applied to development of a low-temperature high-sensitivity miniaturized magnetic-field sensor with an extended dynamic range.

I. INTRODUCTION

Optically pumped (atomic) magnetometers are a rapidly developed technology in modern magnetometry. The sensitivity of atomic magnetometers (AMs) has already reached that of superconducting quantum interference devices (SQUIDs) [1]. At the same time, AMs do not require cryogenic temperature and consume significantly less power compared to SQUIDs. Atomic magnetometers have already found promising applications in medicine for magnetocardiography [2], magnetoencephalography [3], magnetomyography [4], blood velocimetry [5], etc. They can also be used in biology for studying plant biomagnetism [6] or observing nuclear magnetic resonances in biomolecules [7].

One of the most robust and simple techniques in atomic magnetometry is based on the ground-state Hanle effect (GSHE) linked with the zero-field level-crossing phenomenon

[8–10]. In contrast to the excited-state Hanle effect studied by Hanle [11] and his contemporaries, the GSHE provides a much narrower level-crossing resonance (LCR), especially if a buffer gas or an antirelaxation coating of the cell walls is used. This feature immediately suggested to researchers an application of the effect for measuring very weak magnetic fields [12,13]. First studied in cadmium vapors [14], the GSHE is nowadays used in quantum magnetometry mainly with He or alkali-metal vapors such as Rb, Cs, and K.

A single circularly polarized light wave is usually used in GSHE-based sensors to both pump atoms and probe their quantum state. To observe a nonlinear resonance in the light wave intensity transmitted through the vapor cell, the transverse magnetic field is slowly ($\lesssim$200 Hz) scanned around zero. This technique does not require the additional rf magnetic field as in several other types of AMs [15,16], simplifying the scheme and mitigating crosstalk problems between adjacent sensor heads in a multichannel mode of operation. The simplicity of the scheme also provides an opportunity for radical miniaturization of the sensor while

*Corresponding author: brazhnikov@laser.nsc.ru

013113-1

maintaining high reliability and sensitivity of the measurement [17,18].

State-of-the-art Hanle sensors [2–4,17–19] engage the spin-exchange relaxation-free (SERF) regime [20] to reduce the linewidth of the resonance. This helps achieve the highest sensitivity (the smallest detectable change in the magnetic field [16,21]) through a simple relation $\delta B \approx \triangle / \mathcal{S}$, where $\triangle$ is the full width at half maximum (FWHM) of the resonance (in gauss units) and $\mathcal{S}$ is the signal-to-noise ratio (SNR) in a 1-Hz bandwidth. The SERF regime, however, requires a high atomic density, i.e., an increased alkali-metal vapor temperature, which is usually well above $100\,^{\circ}\text{C}$. It also means relatively high power consumption and heat release of the sensor, especially in a multichannel mode used in several medical applications.

As a further development of the GSHE-based sensing technique, it would be interesting to propose a technique that can provide a high sensitivity of measurements at a much lower temperature of vapors ($T \lesssim 60\,^{\circ}\text{C}$) in a small vapor cell ($V \ll 1\ \text{cm}^3$). Reducing the linewidth of the resonance without the SERF regime, a high sensitivity of the sensor can be obtained by increasing the SNR. Since it is proportional to the resonance contrast C, there is a problem of increasing C or, more precisely, the contrast-to-width ratio (CWR) of the zero-field LCR under a low-temperature regime.

At low temperature the standard Hanle scheme with a single circularly or linearly polarized light wave can only demonstrate high contrast and/or high CWR resonances for extended vapor cells ($V \gg 1\ \text{cm}^3$) [22–27], making it difficult to design a miniature sensor. Other types of AMs based on nonlinear Faraday rotation also require a relatively large vapor cell volume to achieve subpicotesla sensitivity at low vapor temperatures [28,29]. Various pump-probe cw [30–35] or pulsed [36–38] light-field configurations can help us overcome this problem. For example, high-quality Hanle resonances were recently observed in our pump-probe scheme with cesium vapors [35]: $C \approx 80\%$ was achieved at $\triangle \approx 2\ \text{mG}$, yielding a large CWR of around $40\%/\text{mG}$. The light field was composed of two counterpropagating light waves of circular polarizations with opposite handedness (σ^+-σ^- configuration). Since a small ($5 \times 5 \times 5\ \text{mm}^3$) cubic vapor cell was used, the scheme is attractive for the development of a highly sensitive miniaturized magnetic-field sensor. A key advantage of the studied scheme consisted in the possibility of obtaining high-quality resonances at low vapor temperatures ($T \leqslant 60\,^{\circ}\text{C}$).

Although linearly and circularly polarized light beams are mainly used in atomic magnetometers, there are several pump-probe schemes with elliptically polarized single beams that have been successfully applied to magnetic-field sensing. For example, in [39] an elliptically polarized off-resonant laser beam and a miniature ($5 \times 5 \times 5\ \text{mm}^3$) Rb vapor cell were used. A zero-field LCR was observed in the rotation of the polarization ellipse caused by the circular birefringence of the medium. To achieve a sensitivity of $7\ \text{fT}/\sqrt{\text{Hz}}$, the SERF regime was engaged. This technique has subsequently been developed to perform vector measurements under the near-zero-field condition [40]. A polarization modulation Bell-Bloom-like scheme was investigated in [41]. The authors used a centimeter-scale ($2 \times 2 \times 5\ \text{cm}^3$) Rb vapor

cell to observe the coherent-population-trapping (CPT) resonances in the light wave transmission. The cell was heated to a relatively low temperature of $78\,^{\circ}\text{C}$. Based on the provided contrast and linewidth measured values, the authors deduced a picotesla sensitivity of their technique. Another simple and efficient scheme with time-modulated ellipticity of the light wave was proposed in a recent study using a Cs vapor cell of $8 \times 8 \times 8\ \text{mm}^3$ [42]. The resonant circular component of light was used to pump atoms into a so-called stretch Zeeman state, while the linear component was used to measure optical rotation induced by circular birefringence of the medium due to off-resonant interaction with the pumped atoms. The cell was heated to a temperature of $90\,^{\circ}\text{C}$ and a sensitivity of $15\ \text{fT}/\sqrt{\text{Hz}}$ was achieved. Another single-beam pulsed (push-pull) scheme was studied in [36] that could provide high sensitivity at a temperature of Cs vapors as low as $20\,^{\circ}\text{C}$. The cell was a 30-mm-diam evacuated paraffin-coated glass bulb.

The resonant interaction of ^{87}Rb atoms with a single light wave with ellipticity only slightly different from 45° was studied in [43]. Such a wave can be decomposed into a relatively strong pump wave and a weak probe wave with counterrotating circular polarizations (here referred to as σ^+ and σ^- components). The transmission of the probe wave was monitored separately using a polarimeter. The relatively low pressure of the buffer gas (25 Torr) allowed the authors to excite a single optical transition $F_g = 2 \rightarrow F_e = 2$ in the D_1 line and observe a LCR of electromagnetically induced transparency (EIT) type in a centimeter-scale low-temperature ($62\,^{\circ}\text{C}$) vapor cell. However, to achieve the 25% resonance contrast, a microwave field was required, meaning that a bulky microwave cavity had to be used. A similar low-temperature technique, without a microwave field, was used then to demonstrate a three-axis AM with a sensitivity of approximately $10\ \text{pT}/\sqrt{\text{Hz}}$ in a centimeter-size Rb vapor cell [44].

Here, inspired by the results in the σ^+-σ^- cw configuration [35], we consider a scheme that employs only a single resonant elliptically polarized wave instead of using two counterpropagating waves. Similarly to the scheme studied in [43,44], such a wave can be decomposed into the probe E_p and pump E_c circularly polarized components σ^+ and σ^-. The probe-wave transmission is monitored on the polarimeter. The experiments show that the same high-quality resonances can be observed in the proposed single-beam scheme with a low-temperature $5 \times 5 \times 5\ \text{mm}^3$ Cs vapor cell as in the two-beam σ^+-σ^- configuration. Obviously, such a scheme with only one beam is much more attractive for creating a miniature sensor. Besides, the scheme provides an additional possibility for differential observation of the pump- and probe-wave transmission signals with the help of a balanced photodetector, suppressing some types of noise similarly to schemes with a polarization rotation [17,39,42].

It should be noted that, compared to the single-beam scheme proposed in [43], we observe electromagnetically induced absorption (EIA) resonance in the transmission of the probe wave instead of EIT resonance. This is due to the relatively high buffer-gas pressure in the cell, where both optical transitions $F_g = 4 \rightarrow F_e = 3$ and $F_g = 4 \rightarrow F_e = 4$ in the D_1 line are excited by light, allowing us to observe extremely high contrast ($\gtrsim 80\%$) of the resonance without the need to

apply a microwave field as in [43]. Preliminary measurements of the noise spectrum density reveal a 1.8 pT/$\sqrt{\text{Hz}}$ sensitivity of measurements. However, an estimated shot-noise-limited sensitivity is around 60 fT/$\sqrt{\text{Hz}}$, which can be achieved after applying additional efforts to reduce various noise sources in our scheme, in particular, relative intensity noise of the laser radiation, magnetic-field noise due to insufficient magnetic shielding of the cell, and other technical noises mainly in electronics.

Finally, we have developed a simplified theoretical model that allows us to obtain explicit analytical solutions of the resonance line shape over a wide range of pump-wave intensities, i.e., beyond the perturbation theory approach that is commonly used in other works. This model predicts a line-narrowing effect caused by transition openness (Sec. II). The effect is confirmed by experiments (Sec. III B). We note that LCRs of the EIA type have been rarely used in atomic magnetometry (see, e.g., [45,46]). One of the main reasons is that EIA resonances usually exhibit a much worse contrast-to-width ratio compared to EIT resonances. In Sec. III C we demonstrate that the proposed scheme eliminates this drawback and therefore expands the scope of EIA applications.

II. THEORY

Electromagnetically induced transparency or absorption effects are usually observed in atomic vapors as subnatural-width resonances either in a single-frequency magneto-optical (Hanle) configuration [47,48] or in a two-frequency light field [49,50]. The resonance sign (EIT or EIA) depends on different experimental conditions, such as the structure of the energy levels involved in combination with the polarization of the light wave and the direction (transverse or longitudinal) of the magnetic-field vector scan or the presence of a residual magnetic field (in the Hanle configuration) [23,50–55], collisional depolarization of the excited state in buffered or antirelaxation-coated vapor cells [52,56–58], etc.

Doppler line broadening or buffer-gas-collision broadening can also affect the resonance sign due to the mutual influence of neighboring optical transitions in the D_1 or D_2 lines in alkali-metal atoms [23,25,50,54,59]. For instance, in [43] the excitation of a single optical transition $F_g = 2 \rightarrow F_e = 2$ in the D_1 line of ^{87}Rb by an elliptically polarized light wave led to observation of the well-known EIT effect in the probe (σ^-) wave transmission as the result of destructive interference of the σ^+ and σ^- optical transitions [60]. In our scheme, in contrast, we observe the EIA effect in the D_1 line of Cs under similar conditions. This resonance behavior can be explained by a significant overlap between the transitions $F_g = 4 \rightarrow F_e = 3$ and $F_g = 4 \rightarrow F_e = 4$ that are not resolved spectroscopically at 130 Torr neon used as a buffer gas [the scheme of levels is shown in Fig. 1(a)]. The interference terms of these two transitions have opposite signs due to properties of the Clebsch-Gordan coefficients [61], leading to significant suppression of the σ^+-σ^- interference effects when the transitions are completely overlapped.

In our analysis, therefore, we consider the two circularly polarized components of the light field as independent, the probe wave $\mathbf{E}_p(t, z)$ and the pump (coupling) wave $\mathbf{E}_c(t, z)$, traveling along the z axis. In the Λ-scheme model, the light
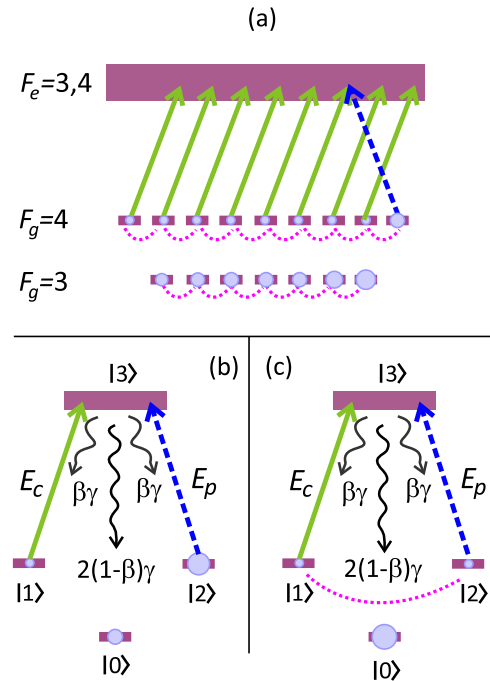

FIG. 1. (a) Scheme of energy levels in the D_1 line of Cs. The hyperfine structure in the upper state is not resolved due to buffer-gas-collisional broadening. The Zeeman sublevels of the upper state are not shown. Green solid and blue dashed arrows stand for the pump and the probe waves, respectively (for simplicity, we show only one σ^- transition for the probe light). Pink dotted lines in the two ground-state levels denote Zeeman coherences induced by the transverse magnetic field. Circles schematically reflect the sublevel populations. A simplified three-level model of the atom is shown (b) in the absence of the transverse magnetic field and (c) in the presence of the field. See the text for further details

field is commonly considered as scalar, where $\mathbf{E}_c(t, z)$ and $\mathbf{E}_p(t, z)$ drive the $|1\rangle \rightarrow |3\rangle$ and $|2\rangle \rightarrow |3\rangle$ transitions, respectively, without reference to the wave polarizations [Figs. 1(a) and 1(b)]. Therefore, the light field can be written as

$$E(t, z) = E_c(z)e^{-i\omega t} + E_p(z)e^{-i\omega t} + \text{c.c.}, \qquad (1)$$

where $E_{c,p}(z)$ are the real amplitudes slowly varying in space, ω is the optical frequency, and c.c. means the complex conjugate terms. We assume that the buffer-gas broadening prevails over the Doppler broadening, so atomic motion can be neglected. This explains the absence of e^{ikz} terms in (1) with k the absolute value of the wave vector.

All optical transitions in the D_1 line are open. In our experiments, the field (1) is in resonance with two of them, namely, $F_g = 4 \rightarrow F_e = 3, 4$ [Fig. 1(a)]. Qualitative explanations for the reasons leading to observation of high-contrast EIA resonances in a probe-wave transmission can be found in [35]. Here we consider a simplified three-level (Λ) scheme that, on the one hand, provides a similar explanation and, on the other hand, allows us to derive explicit analytical solutions valid for a wide range of the pump-wave intensities. In the scheme shown in Figs. 1(b) and 1(c), $|3\rangle$ is the excited state, while $|1\rangle$ and $|2\rangle$ are the ground-state sublevels of the same energy. These levels are in resonance with the light field. The trap state $|0\rangle$ is not in resonance with the field and only serves

to collect atoms as a result of their spontaneous decay from the excited state. For simplicity, it is assumed that the dipole moments of the two arms $|1\rangle \rightarrow |3\rangle$ and $|2\rangle \rightarrow |3\rangle$ are the same and equal to d_0. This means that the spontaneous decay rates of these arms are also the same and can be denoted by $\beta\gamma$, with 2γ the total spontaneous relaxation rate of the excited state ($2\gamma \approx 2\pi \times 4.56$ MHz for the Cs D_1 line) and β the branching ratio that controls the degree of openness of the scheme: $0 \leqslant \beta \leqslant 1$, where $\beta = 1$ corresponds to the case of a closed scheme. The ground-state relaxation is governed by the rate Γ, which is usually $\lesssim 1$ kHz in the experiments with alkali-metal atoms in the presence of a buffer gas (it is not shown in the figure for simplicity). Note that such a scheme is commonly used for theoretical study of various manifestations of the EIT effect [62–64] as well as some types of the EIA effect [65,66].

We use a standard quantum-mechanics formalism of the density matrix $\hat{\rho}(z, t)$ to describe the atom-field interaction (for instance, see [67]). The corresponding master equation has the Lindblad form

$$\frac{\partial}{\partial t}\hat{\rho} = -\frac{i}{\hbar}[(\hat{H}_0 + \hat{V}_b + \hat{V}_e), \hat{\rho}] + \hat{\mathcal{R}}\{\hat{\rho}\}, \qquad (2)$$

where the term in square brackets is the commutation operation of two matrices, $\hat{H}_0$ is part of the total Hamiltonian for a free atom, and $\hat{V}_b$ and $\hat{V}_e$ describe the interaction between the atoms and the magnetic and light fields, respectively (in the electric dipole approximation). The linear functional $\hat{\mathcal{R}}$ is responsible for the relaxation processes in the atom. Details can be found in the Appendix.

We assume the probe wave to be weak enough so that optical properties of the medium do not depend on E_p, the linear approximation with respect to the probe field. In the experiments, a photodetector registers the wave intensity $I_{p,c} = (c/2\pi)E_{p,c}^2$, with c the speed of light. We first analyze the LCR in the pump-wave intensity, which obeys the equation (see the Appendix)

$$\frac{dI_c}{dz} = -\alpha_c I_c. \qquad (3)$$

Here the pump-wave absorption index is

$$\alpha_c \approx \frac{3\gamma\beta\lambda^2 n_a}{4\pi\gamma_{eg}}\rho_{11}, \qquad (4)$$

where ρ_{11} is the population of sublevel $|1\rangle$; λ is the light wavelength (approximately equal to 894.5 nm for the Cs D_1 line); n_a is the atomic number density, which is strongly dependent on the vapor temperature; and γ_{eg} is the relaxation rate of the optical coherences in the Λ scheme, determining the linewidth of the optical transitions, $\gamma_{eg} = \Gamma + \gamma + \gamma_c$, with γ_c the rate of dephasing collisions between the cesium atoms and the buffer-gas atoms. In our experiments, the collisional line broadening significantly prevails over the other impacts, i.e., $\gamma_c \gg \gamma, \Gamma$, meaning $\gamma_{eg} \approx \gamma_c$.

In the linear regime on the probe wave, the absorption index α_c depends only on the pump-wave intensity I_c, which in turn slowly varies along the z axis due to absorption in the cell. However, as we will see, the pump wave experiences low absorption in the cell, i.e., the medium is optically thin for this wave (in the considered temperature of the cell). Therefore,

α_c depends on I_c as a constant parameter. This approximation allows us to obtain a simple solution in the form of the well-known Beer-Lambert-Bouguer law

$$I_c(z) = I_{c0}e^{-\alpha_c z}, \qquad (5)$$

with I_{c0} the pump-wave intensity at the entrance of the cell. For theoretical analysis, it is convenient to define a dimensionless coefficient of transmission following the expression

$$\eta_c = \frac{I_c(z = L_{\text{cell}})}{I_{c0}} = e^{-\alpha_c L_{\text{cell}}}, \qquad (6)$$

where L_{cell} is the cell length.

Substituting ρ_{11} from the Appendix into (4), we get a compact solution

$$\alpha_c \approx \frac{\alpha_0(1 + \xi + 4\Omega^2\tau^2)}{(1 + \xi)[1 + (2 - \beta)\xi] + 4[1 + (1 - \beta)\xi]\Omega^2\tau^2}. \qquad (7)$$

Here $\Omega = gB_x$ is the Larmor frequency, where g is the gyromagnetic ratio (approximately equal to $2\pi \times 350$ Hz/mG for the Cs ground state), B_x is the transverse magnetic-field strength, $\tau = \Gamma^{-1}$ is the relaxation time of the ground state, and ξ is the modified saturation parameter

$$\xi = \frac{R_c^2\tau}{\gamma_{eg}} = \frac{3\beta\gamma\tau\lambda^3}{16\pi^2\hbar c\gamma_{eg}}I_c, \qquad (8)$$

which is nothing but the optical pumping rate R_c^2/γ_{eg} multiplied by the time of coherent interaction τ, where $R_c = d_0 E_c/\hbar$ is the Rabi frequency for the pump field. In (8) we have taken into account the relation $\beta\gamma = 4k^3 d_0^2/3\hbar$.

The coefficient α_0 in (7) is the absorption index at the center of the resonance curve ($\Omega = 0$) in the low-intensity limit ($\xi \ll 1$)

$$\alpha_0 = \frac{3\beta\gamma\lambda^2 n_a\rho_0}{4\pi\gamma_{eg}}, \qquad (9)$$

with ρ_0 the initial population of a sublevel in the ground state. In our model, we take $\rho_0 = \frac{1}{3}$ for each of the sublevels $|0\rangle$, $|1\rangle$, and $|2\rangle$.

The other approximations of the theory that should be mentioned are the following. We neglect the effect of optical line splitting that can be observed when $\Omega \sim \gamma_{eg}$, because under our experimental conditions the resonance width is significantly less than γ_{eg}, so we can focus on the range of $\Omega \ll \gamma_{eg}$. We can also consider the condition $R_c^2 \ll \gamma_{eg}\gamma$ to be fulfilled for a reasonable light wave intensity. The condition $\gamma\tau \gg 1$ is also satisfied in the presence of a buffer gas when the coherent interaction time between light and atoms increases considerably compared to the case of a vacuum vapor cell. Finally, since we neglected any interference effects between the probe and the pump waves, the subnatural-width-resonance splitting effect [63,68,69] does not occur.

Figure 2(a) shows the behavior of $\alpha_c(\Omega)$ calculated for typical experimental conditions at $\beta = 1$ and 0.5. Figure 2(b) demonstrates the corresponding transmission coefficient $\eta_c(\Omega)$. The EIT resonance is observed with significantly suppressed height in the case of an open system of levels ($\beta = 0.5$). The pump-wave absorption is low at both $\Omega = 0$ and $\Omega \neq 0$, especially if the system is open. It validates our
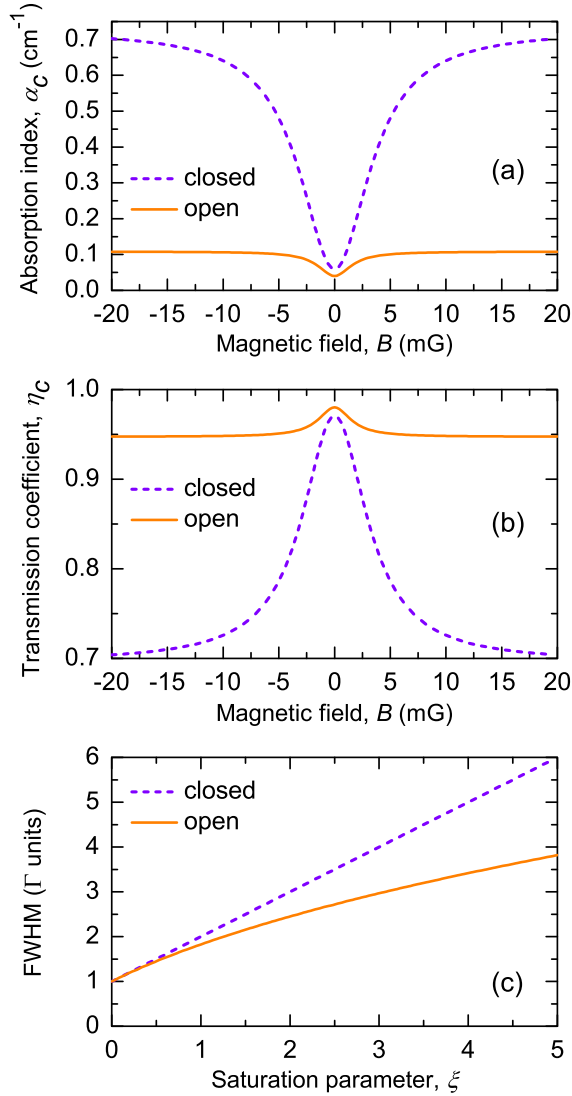
FIG. 2. Calculated zero-field level-crossing resonance of EIT for (a) the pump-wave absorption index and (b) the transmission coefficient in closed ($\beta = 1$) and open ($\beta = 0.5$) systems of energy levels. (c) Full width at half maximum of the resonance as a function of light wave intensity (dimensionless saturation parameter). The parameters of the calculation are $2\gamma = 2\pi \times 4.56\,\text{MHz}$, $\Gamma = 10^{-4}\gamma$, $\gamma_c = 2\pi \times 2\,\text{GHz}$, $n_a = 10^{12}\,\text{cm}^{-3}$, $\lambda = 894.5\,\text{nm}$, and $L_{\text{cell}} = 0.5\,\text{cm}$. In (a) and (b) the Rabi frequency $R_c = \gamma$.

approximation concerning the low pump-wave absorption in the cell.

The function $\alpha_c(\Omega)$ has the Lorentzian-like shape. The low pump-wave absorption means that $\eta_c(\Omega)$ is also described by the same line shape due to the approximation

$$\eta_c(\Omega) \approx 1 - \alpha_c(\Omega)L_{\text{cell}}. \tag{10}$$

The resonance linewidth (FWHM) in $\alpha_c(\Omega)$ and $\eta_c(\Omega)$ can be easily figured out from (7):

$$\Delta_c \approx \Gamma \sqrt{(1 + \xi)\left(1 + \frac{\xi}{1 + (1 - \beta)\xi}\right)}. \tag{11}$$

The effect of openness-induced line narrowing readily follows from the expression (11). Indeed, if the system of levels is closed ($\beta = 1$), then one gets a linear behavior $\Delta_c \approx \Gamma + R_c^2/\gamma_{eg} \propto I_c$. Such a dependence is well known in the theory of GSHE [20,70] as well as in the theory of two-frequency EIT or CPT effects [71,72] for homogeneously broadened closed transitions. In particular, the latest analytical results for a real (degenerate) structure of energy levels can be found in [73]. Otherwise, in open systems ($\beta < 1$), the linewidth demonstrates a square-root-like behavior $\Delta_c \propto \sqrt{I_c}$, which is clearer at $\xi \gg 1$. Similar behavior can be extracted from the linewidth expression in [74] for two-frequency CPT resonances in a buffered vapor cell. We demonstrate this narrowing effect in Fig. 2(c). This openness-induced line-narrowing effect is not emphasized in the literature for magneto-optical (GSHE) resonances, nor has it attracted much attention as a separate line-narrowing effect in two-frequency CPT experiments.

The resonance contrast can be defined as $C = 100\% \times [\eta_c(0) - \eta_c(\infty)]/\eta_c(0)$ where $[\eta_c(0) - \eta_c(\infty)]$ is the resonance height and $\eta_c(\infty)$ means the background, i.e., the light transmission at $\Omega \gg \Delta_c$. As seen in Fig. 2(b), in the standard Hanle configuration with only one circularly polarized wave for pumping and probing, the resonance contrast is quite low (less than 5%) for a temperature less than or equal to 60 °C. The large difference between the resonance heights in closed and open systems [dashed and solid curves in Figs. 2(a) and 2(b)] can be easily explained. Indeed, at $\Omega = 0$ [Fig. 1(b)], the pump wave experiences low absorption in the cell due to optically pumping most of the atoms to the noninteracting state $|2\rangle$ (in the closed scheme) or to both noninteracting states $|2\rangle$ and $|0\rangle$ (in the open scheme). The probe light is assumed to have such a weak strength that it does not noticeably affect the sublevel populations. Then, if the system of levels is closed and $\Omega \gg \Delta_c$, the two sublevels $|1\rangle$ and $|2\rangle$ are strongly mixed, i.e., the so-called Zeeman coherence is created [pink dotted line in Fig. 1(c)]. Such a mixing prevents the optical pumping of the $|2\rangle$ sublevel and leads to a considerable scattering of the pump-wave light. Therefore, we can see a relatively large amplitude of the EIT resonance in the case of a closed scheme [solid curves in Figs. 2(a) and 2(b)]. Otherwise, openness of the scheme leads to a low absorption even when $\Omega \gg \Delta_c$ because most of the atoms are collected in the $|0\rangle$ trap sublevel by means of optical pumping [Fig. 1(c)].

In [25] the authors proposed to overcome a problem with low contrast of EIT resonance in the standard Hanle scheme by using potassium vapors instead of cesium. That was made possible due to a small energy separation between the ground-state hyperfine levels in K, leading to a higher absorption at $B \neq 0$ than in the case of Cs. In a sense, the system of levels in potassium can be considered as closed. However, a K vapor cell requires either an extended length (greater than or equal to 5 cm) or a higher temperature of vapors to achieve a good resonance contrast. Another way is typically realized in miniature SERF magnetometers where very high buffer-gas pressure is used (1 atm and more), leading to overlapping of the ground-state hyperfine levels in Cs or Rb atoms [17,20]. However, an increased temperature (greater than or equal to 150 °C) is also required to obtain a desirable contrast.

Here we study the possibility of a significant increase in the resonance contrast at lower temperatures (less than or equal

to 60 °C) by means of adding the second (probe) light wave. Such pump-probe light-field configurations have been studied in several works, expanding the capabilities of the standard Hanle scheme. Most of them utilize two separate light waves [31–35,37,38,75–77]. However, it is obvious that a single light wave configuration is preferable for the development of a miniature magnetic-field sensor. Our current proposal has much in common with the proposal studied in [43]: An elliptically polarized light wave can be treated as two copropagating circularly polarized light waves of opposite handedness. Here, in contrast to [43], we propose to use a higher buffer-gas pressure so that the excited-state hyperfine levels in the cesium D_1 line are overlapped, while the ground-state hyperfine structure is spectroscopically resolved. As we will see, such a condition appears to be a key point of the proposed technique. In addition, the considered scheme allows either monitoring the LCR in each channel of a polarimeter or using a differential signal of two channels, increasing the SNR.

By analogy with (3) and (4), the probe-wave absorption index reads

$$\alpha_p \approx \frac{3\gamma\beta\lambda^2 n_a}{4\pi\gamma_{eg}}\rho_{22}$$

$$\approx \frac{\alpha_0[(1+\xi)(1+2\xi)+4\Omega^2\tau^2]}{(1+\xi)[1+(2-\beta)\xi]+4[1+(1-\beta)\xi]\Omega^2\tau^2}. \quad (12)$$

This function has the same linewidth as $\alpha_c(\Omega)$ according to the expression (11). However, since the transmission coefficient η_p, defined similarly to (6), is monitored in the experiments rather than the absorption index α_p, the GSHE resonance linewidth can slightly differ from (11) because the approximation (10) is not valid for the probe wave.

In contrast to $\alpha_c(\Omega)$, the function $\alpha_p(\Omega)$ exhibits the subnatural-width EIA resonance instead of the EIT resonance [Fig. 3(a)]. This behavior has a clear qualitative explanation. For brevity, consider only the case of an open scheme (orange solid curve in the figure). At $\Omega = 0$, the probe wave experiences an increased absorption in the cell because many atoms have been prepared in the $|2\rangle$ sublevel by the pump field. Now, if $\Omega \gg \Delta_c$, the atoms are mostly transferred to the $|0\rangle$ trap sublevel and the medium becomes almost transparent. This process explains the sign of the resonance as well as its large height in $\alpha_p(\Omega)$.

The transition openness also leads to an increase in the resonance height in the transmission coefficient shown in Fig. 3(b). The behavior of the probe-wave absorption therefore is very different from that of the pump wave [compare Figs. 2(b) and 3(b)]. The additional line broadening due to violation of the condition (10) for the probe wave is seen in Fig. 3(c) at higher pump-wave intensities.

Based on (7) and (12), we can figure out the ratio between the heights A_c and A_p of the resonance in α_c and α_p, respectively. The height can be calculated as the difference $A = |\alpha(\Omega = 0) - \alpha(\Omega \to \infty)|$. A routine procedure leads to the ratio

$$\frac{A_p}{A_c} = 1 + 2(1-\beta)\xi. \quad (13)$$

From this, a constructive action of both the optical pumping process, proportional to ξ, and the openness of the system,
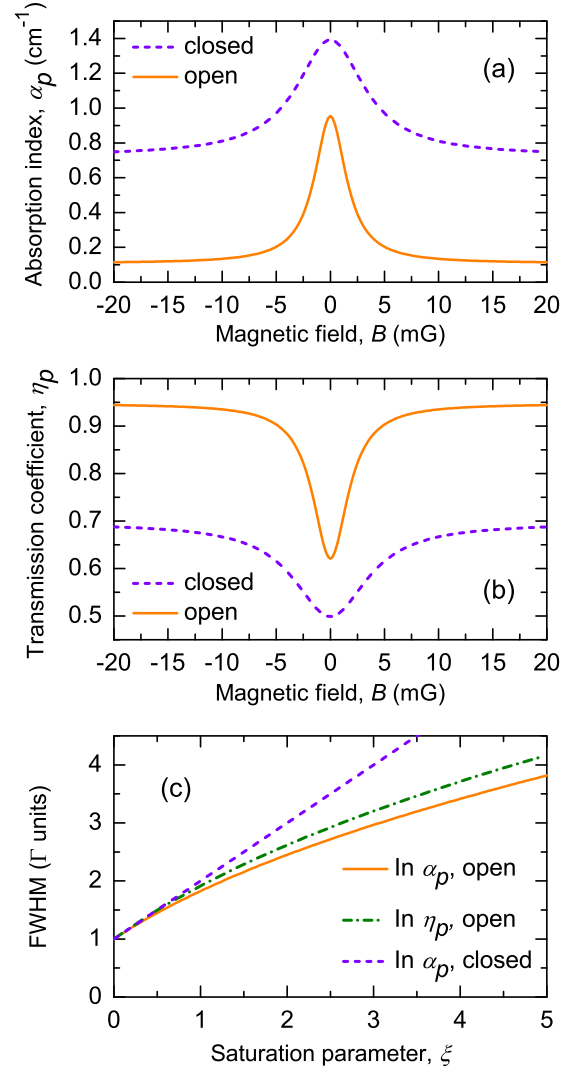

FIG. 3. Calculated zero-field level-crossing resonance of EIA for (a) the probe-wave absorption index and (b) the transmission coefficient in closed ($\beta = 1$) and open ($\beta = 0.5$) systems of energy levels. (c) Full width at half maximum of the resonance as a function of pump-wave intensity, namely, the dimensionless saturation parameter ξ, observed in the absorption index α_p (orange solid curve) and in the transmission coefficient η_p (green dash-dotted curve). The dashed line shows the linewidth behavior (proportional to $1 + \xi$) in the closed system of levels. The parameters of the calculation are the same as in Fig. 2

proportional to $1 - \beta$, on the resonance height can be clearly seen: In an open system of levels ($\beta \neq 1$), the condition $\xi \gg 1$ immediately leads to the relation $A_p \gg A_c$, making the proposed pump-probe scheme much more attractive than the standard Hanle scheme.

The expression (7) for the pump-wave absorption index is valid in a wide range of light intensities. At the same time, the expression (12) is valid only for such a probe-wave intensity that is low enough to not disturb the atomic sublevel populations. Therefore, it is important to figure out an expression for the light intensity that can characterize a degree of the atom-field interaction strength in the case of an open scheme of levels and a finite time of interaction. In a widely used

steady-state two-level model of the atom, such an intensity is known as the saturation intensity

$$I_{\text{sat}2l} = \frac{4\pi^2 \hbar c \gamma_{12}}{3\lambda^3}, \tag{14}$$

with γ_{12} the relaxation rate of the optical coherence in the two-level atom that characterizes the homogeneously broadened line shape of the resonance. This rate considerably exceeds the spontaneous relaxation rate γ in the case of frequent dephasing collisions of alkali-metal atoms with buffer-gas atoms (at $P \gg 1$ Torr). At $I = I_{\text{sat}2l}$, a light-field absorption index in the two-level atom drops to half of its maximum value that takes place at $I \ll I_{\text{sat}2l}$. For the parameters used in our experiments, we can estimate $I_{\text{sat}2l} \approx 340$ mW/cm^2 (versus 1.1 mW/cm^2 in a purely spontaneous relaxation regime [78]).

Obviously, the expression (14) is not applicable to the open Λ scheme considered here. A valid expression can be obtained in the same way as in the two-level model, namely, we use (7) to define saturation intensity as an intensity that satisfies the condition $\alpha_c(I_{\text{sat}}) = \alpha_0/2$. Trivial calculations lead to the expression

$$I_{\text{sat}} = \frac{16\pi^2 \hbar c \Gamma \gamma_{eg}}{3\beta \gamma \lambda^3 (2-\beta)}. \tag{15}$$

This expression can be written in terms of the saturation parameter from (8) as $\xi_{\text{sat}} = (2-\beta)^{-1}$, so in the closed Λ scheme ($\beta = 1$) we simply get $\xi_{\text{sat}} = 1$. This is obvious from (11) because at this value the resonance linewidth starts to suffer from the power broadening. For instance, under the experimental conditions used, we can estimate I_{sat} to be around 0.25 mW/cm^2, which is much less than in the two-level model. Note that the developed theory is adequate, only if $I_p \ll I_{\text{sat}}$. Comparing (8) and (15), we can write an alternative expression for the saturation parameter in our scheme:

$$\xi = \frac{I_c}{(2-\beta)I_{\text{sat}}}. \tag{16}$$

We emphasize once again the positive role of the transition openness in the pump-probe scheme that, on the one hand, shrinks the resonance linewidth and, on the other hand, significantly increases its contrast. It should be noted that it is a unique case because such a transition openness has long been considered as a harmful effect, noticeably degrading properties of both the EIT and EIA resonances in various schemes [23,79–82]. In general, the line-narrowing effect considered contributes to other known narrowing effects of subnatural-width resonances, for instance, due to atomic motion in a gas (Doppler narrowing) [83,84], suppression of spin-exchange relaxation [20,85], and the influence of the transverse intensity distribution of a light beam [86,87].

III. EXPERIMENT

A. Setup

The experimental setup is shown in Fig. 4. We use a distributed Bragg reflector diode laser with a radiation wavelength of $\lambda \approx 894.5$ nm (Cs D_1 line) and a linewidth less than or equal to 0.5 MHz. The laser output beam is passed through a Faraday optical isolator. A set of neutral density filters is used to control the light power. Subsequently, the
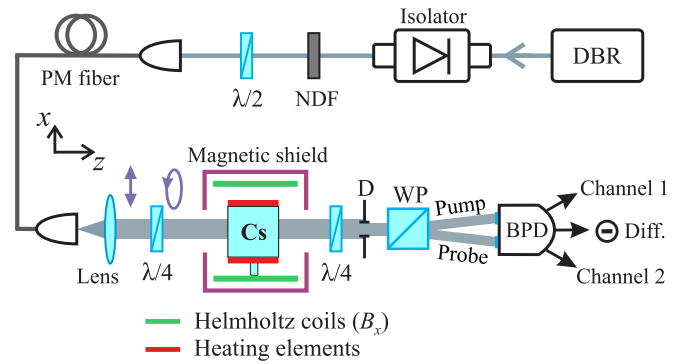

FIG. 4. Experimental setup: DBR, distributed Bragg reflector diode laser; Isolator, optical Faraday insulator; NDF, set of neutral density filters; $\lambda/2$ and $\lambda/4$, phase half waveplate and quarter waveplate, respectively; PM fiber, polarization maintaining fiber; Cs, cesium vapor cell; D, iris diaphragm; WP, Wollaston prism; and BPD, balanced photodetector.

beam is sent to a polarization-maintaining optical fiber. A half waveplate ($\lambda/2$) before the fiber is used to adjust the linear polarization of the beam. A lens is placed after the fiber to collimate the beam (another lens is included in the fiber collimator and can be moved). The beam diameter ($1/e^2$) after the lens is around 1.5 mm. A quarter waveplate ($\lambda/4$) placed after the lens creates two circularly polarized light waves, the pump and the probe beams. The relative strength of the beams is determined by the light wave ellipticity and can be controlled by the angle between the main axis of the plate and the direction of linear polarization of the initial light wave (with accuracy reaching approximately 0.1°). For instance, this angle equals 45° if one needs a circularly polarized wave as in the standard Hanle scheme. The pump and probe beams pass through the cesium vapor cell and their circular polarizations are transformed back into the linear polarizations by the second quarter waveplate. Since the circularly polarized pump and probe beams have an opposite handedness, their linear polarizations after the second $\lambda/4$ plate are mutually orthogonal. The beams can then be separated in space by means of a Wollaston prism (WP) and monitored independently by using a balanced photodetector. An iris diaphragm before the WP, having about the same diameter as the beams, is used to reduce the influence of a Gaussian profile of the beam intensity, on the one hand, and helps to slightly improve the resonance contrast, on the other hand (see details in [34]).

A cubic $5 \times 5 \times 5$ mm^3 cesium vapor cell is made of Pyrex glass and filled with a neon buffer gas (approximately equal to 130 Torr). The cell is heated by an ac electric current (100 kHz) applied to resistive heating elements. The elements are made of a polyimide film, containing microwires that carry electric currents in opposite directions to reduce the stray magnetic field. The heating process does not have a visible effect on the LCRs. A three-layer μ-metal magnetic shield is utilized to reduce the ambient field down to approximately 0.1 mG in the cell volume.

The absorption profiles corresponding to the separate optical transitions $F_g = 4 \to F_e = 3$ and $F_g = 4 \to F_e = 4$ are significantly broadened due to collisions with a buffer gas, so they merge into a single absorption line. The laser frequency

is tuned manually to the center of this curve. We use a pair of Helmholtz coils to produce a transverse magnetic field, here referred to as B_x. It is scanned around zero to observe the GSHE resonance.

Let us provide several estimations to check that our experimental conditions meet the main limitations underlying our theory. At $T \approx 60\,^\circ\mathrm{C}$, the atomic number density in the cell (n_a) is around 10^{12} cm^{-3} [78]. Using the well-known expressions [88,89] and coefficients from [90], we get an estimation for the ground-state relaxation rate Γ to be around $2\pi \times 420$ Hz (or approximately 1.1 mG in the magnetic-field domain). The D_1 line broadening data from [91] lead to $\gamma_{eg} \approx 2\pi \times 680$ MHz. In our experiments, the pump-wave intensity is in the range approximately equal to 10–700 mW/cm^2. Therefore, from (8) we can easily deduce that R_c is in the range approximately equal to $2\pi \times (3\text{–}24)$ MHz $\approx (1\text{–}10)\gamma$. For the latter estimation we took $\beta = 0.5$. Finally, in the next section we will see that the LCR lies in the region $B_x \lesssim 50$ mG, i.e., $\Omega \leqslant 2\pi \times 18$ kHz. The estimations provided demonstrate that the following conditions necessary for the validity of our theory are met with a good margin: $\Gamma \ll \gamma \ll \gamma_{eg}$ and $\Omega \ll \gamma_{eg}$. Another condition $R_c \ll \gamma_{eg}\gamma$ can be rewritten as $I_c \ll \gamma(2 - \beta)I_{\mathrm{sat}}/\Gamma \approx 1.5 \times 10^3$ mW/cm^2. Therefore, we can anticipate achieving good agreement between the theory and the experiments at $I_c \lesssim 200$ mW/cm^2.

B. Openness-induced line-narrowing effect

First, we register a GSHE resonance in the standard Hanle scheme where the light wave has circular polarization. At this regime, the laser beam completely transferred to channel 1 of the balanced photodetector (see Fig. 4). At an optical power of 600 μW, the resonance FWHM is around 3.5 mG and the contrast is approximately equal to 12% [Fig. 5(a)], which is defined as $C = (A/B) \times 100\%$, with A the resonance height and B the light transmission at the center of the resonance.

Figure 5(b) shows the dependence of the resonance linewidth on the laser beam intensity. In the figure, the green solid curve fits the experimental data (violet circles) according to the theoretically predicted square-root-like law $\Delta_c \approx \Gamma\sqrt{1 + I_c/I_0}$. Note that our theory is based on a simplified Λ scheme of levels; therefore, we cannot anticipate quantitative agreement between the theory and experiments without using any fitting (free) parameters. Since we have already estimated Γ to be around 1.1 mG, we can use only one fitting parameter $I_0 \approx 5.3$ mW/cm^2. As seen from Fig. 5(b), an increase in the cell temperature leads to an additional broadening that looks like a linearization of the linewidth behavior (orange squares) as mentioned in Sec. II [see Fig. 3(c)]. In addition, in Sec. II we also noted that our expressions are valid if I_c is less than 200 mW/cm^2. Consequently, this can be the reason for the slight deviation from the square-root law in Fig. 5(b) when I_c exceeds this value. In general, we can conclude that both sets of experimental data points in Fig. 5(b) visibly deviate from a linear dependence (dashed line), which could be expected for the closed scheme of energy levels, $\Delta = \Gamma(1 + I_c/I_0)$, i.e., the predicted linewidth narrowing effect is clearly seen in the figure.

Figure 6(a) shows the levelcrossing EIA resonance observed in channel 2 of the balanced photodetector (PD) when
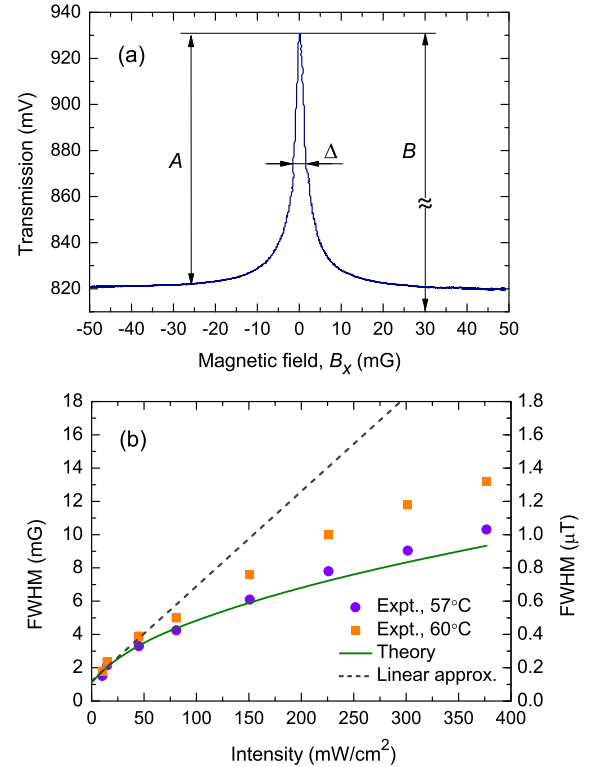

FIG. 5. (a) Level-crossing resonance in the standard Hanle scheme at $P_c \approx 600\ \mu$W and $T \approx 60\,^\circ$C. (b) Linewidth (FWHM) of the resonance versus the wave intensity. The green solid line is a square-root fitting of the experimental data points (violet circles) at a lower temperature of $57\,^\circ$C. Orange squares stand for the FWHM at an increased temperature. The black dashed line is a linear law drawn through the first three experimental points by the method of least squares.

the polarization of the initial beam differs slightly from circular polarization ($\epsilon \approx 41^\circ$). In the case of EIA resonance, the contrast is defined as $C = (A/B) \times 100\%$, where A is the resonance height and B is the background light transmission. As seen in the figure, at 650 μW of the total optical power, the resonance has approximately 80% contrast and a 4 mG linewidth. In contrast to the EIT resonance in the pump-wave transmission (at channel 1), the EIA linewidth behavior is almost linear [Fig. 6(b), violet curve with closed squares]. This differs from the linear law only at $I_t \lesssim 50$ mW/cm^2. This peculiarity can be explained by the fact that the probe-wave intensity is not as low as it is required by the developed theory. Indeed, it changes as the total intensity I_t changes. In particular, the probe-wave intensity can be calculated as $I_p = I_t \sin^2(\epsilon - \pi/4)$, so at $I_t = 50$ mW/cm^2 and $\epsilon = 39^\circ$ we get $I_p \approx 0.25$ mW/cm^2. This value coincides with the saturation intensity (see Sec. II); therefore, the probe wave can be considered to be small in a whole range of I_t. The green solid line with open squares in Fig. 6(b) corresponds to the case when the probe-wave intensity is kept low enough by adjusting the ellipticity of light polarization every time the total intensity is increased (I_p is in the range approximately equal to 40–60 μW/cm^2 for this case). We use a few initial data points to make a linear fit of the experimental data (pink

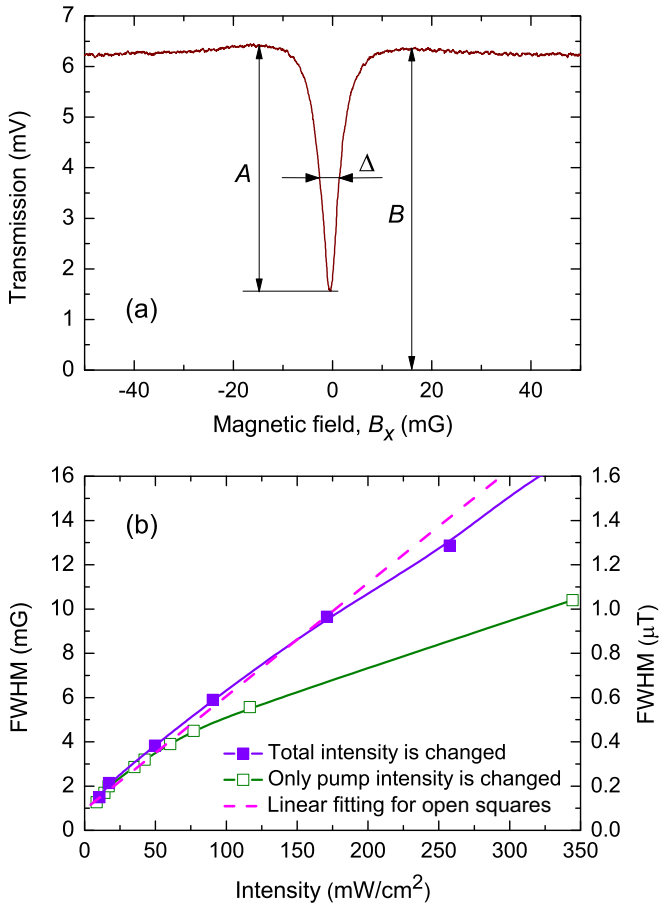FIG. 6. (a) Level-crossing EIA resonance observed in channel 2 of the PD at $\epsilon = 39°$, $P_t = 650\ \mu$W, and $T = 60\ °$C. (b) Linewidth (FWHM) of the resonance as the total light intensity is changed (closed squares) or only the pump-wave intensity is changed (open squares). Solid curves are just guides for the eye. The pink dashed line is the linear fitting for the first six open squares.

dashed line). The square-root-like behavior is now clearly manifested as it has been predicted by the theory.

C. Measurement of the resonance parameters

Here we focus on analyzing the EIA resonance parameters (linewidth, contrast, and contrast-to-width ratio) depending on the total intensity and the ellipticity parameter, keeping the cell temperature around $60\ °$C. As seen in Fig. 7(a), if the light wave polarization differs significantly from the circular polarization (blue triangles and violet asterisks), the linewidth experiences an additional broadening. In this case, the probe-wave intensity is not low enough and the conditions for observation of the EIA resonance are not optimal. The same reason leads to a degradation of the EIA resonance contrast with the intensity increase in Fig. 7(b). At the same time, at $35° < \epsilon < 45°$ (orange squares, pink circles, and green rhombuses), the contrast does not experience a visible degradation with the intensity increase, reaching 83% (orange squares).

The EIA resonance in the probe-wave transmission can be used for magnetic-field measurements. In miniaturized
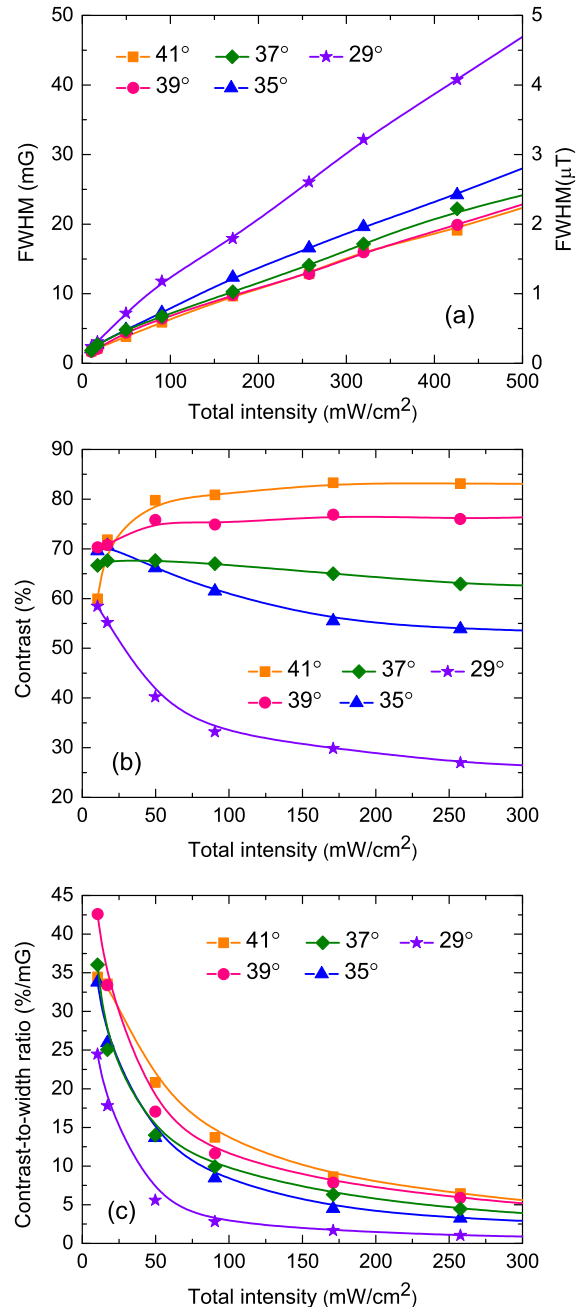

FIG. 7. Parameters of the EIA resonances for different ellipticities versus the total light intensity: (a) linewidth, (b) contrast, and (c) contrast-to-width ratio. Here $T = 60\ °$C. Solid curves are just guides for the eye.

sensors, the noise voltage at the PD is often higher than the photon-shot-noise limit and contains different contributions proportional to the light intensity. In this case, the sensitivity of the measurement depends considerably on the contrast-to-width ratio (CWR) of the resonance, which can be regarded as a figure of merit (see, e.g., [38]). As seen in Fig. 7(c), the EIA resonance CWR takes its maximum value at the lower intensities. It can also be seen that the optimal ellipticity is around 40°.

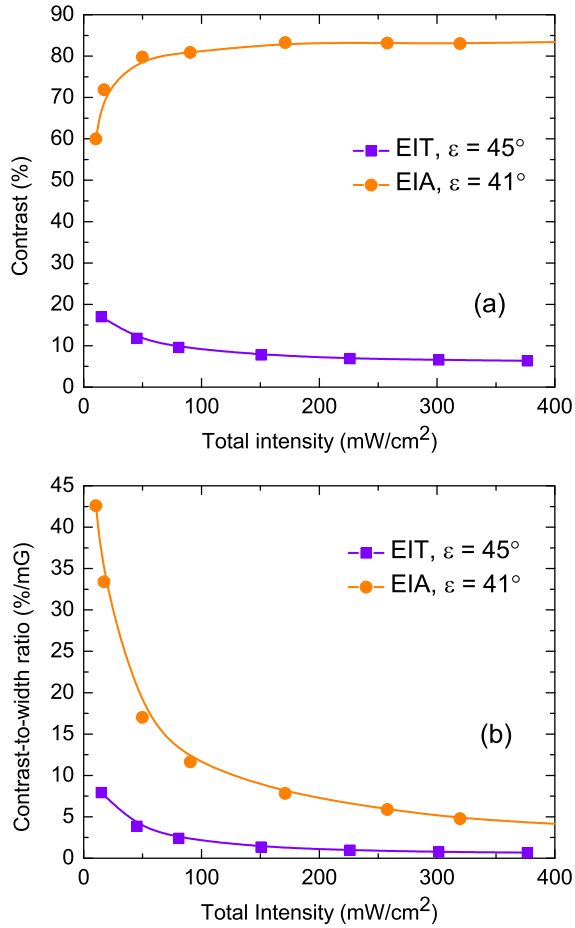Let us compare C and the CWR parameters measured for the EIT (channel 1) and the EIA (channel 2) resonances at

FIG. 8. Comparison of the EIT resonance parameters (in the standard Hanle scheme with a circularly polarized wave) with the best EIA parameters observed in the experiments. Here $T = 60\,°\mathrm{C}$. Solid curves are just guides for the eye.

FIG. 9. Transmission signals observed at $\epsilon = 37°$ in both channels of the balanced PD with simultaneous scanning of the light-field frequency detuning ($f_{\mathrm{scan}} = 0.5\,\mathrm{Hz}$) and the transverse magnetic field ($f_{\mathrm{scan}} = 20\,\mathrm{Hz}$). The separate optical transitions $F_g = 4 \rightarrow F_e = 3$ and $F_g = 4 \rightarrow F_e = 4$ are not resolved due to buffer-gas line broadening. Here $P_t = 5.3\,\mathrm{mW}$ and $T = 63\,°\mathrm{C}$.

the same temperature of the cell. As follows from Fig. 8, the contrast and the CWR are much higher in the case of EIA. The high contrast of the EIA resonances in comparison with the EIT ones is also demonstrated in Fig. 9, where the laser frequency is scanned simultaneously with scanning the magnetic field (spikes correspond to the EIT effect, while dips correspond to the EIA effect). If $B_x \approx 0$, then the pump wave experiences an increased transmission through the cell (EIT), while the probe-wave transmission is dramatically decreased (EIA). We can easily compare the heights of the EIT and EIA resonances. It can be noted that a nonzero optical frequency detuning from the center of absorption line may cause a change in the resonance sign. In this case only one optical transition $F_g = 4 \rightarrow F_e = 3$ or $F_g = 4 \rightarrow F_e = 4$ is predominantly excited by the light, exhibiting EIT- or EIA-type resonances depending on the angular momentum values of the involved levels. In addition, there can be a non-negligible influence of the circular birefringence under a nonzero-frequency detuning, competing with the dichroism effects.

Before we end this section we would like to mention another way to observe the GSHE resonance which consists in monitoring a differential channel at the PD. The pump
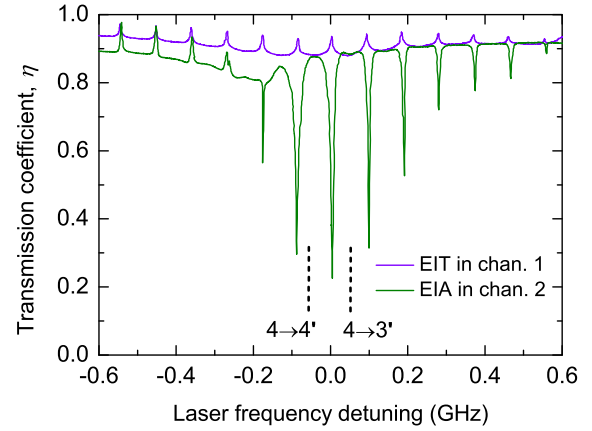
and probe channels provide significantly different magnitudes of the signals. To show them on the same plot, we need to normalized these signals to, for example, the background transmission. Then if we want to include the signal from the differential channel, the background should be extracted from all signals because the differential channel has a zero background. The result of this procedure is demonstrated in Fig. 10. As can be seen, the differential channel provides the resonance with an increased height (solid pink curve) compared to the heights of the EIT and EIA resonances. This observation technique deserves additional study and is not considered in the present paper.

D. Sensitivity

To estimate the sensitivity, we have measured the noise voltage and signal-to-noise ratio in channel 2 at $\epsilon = 37°$ [Figs. 11(a) and 11(b)]. On a log-log plot in Fig. 11(a), the noise decreases linearly down to approximately $30\,\mathrm{nV_{rms}}$ at
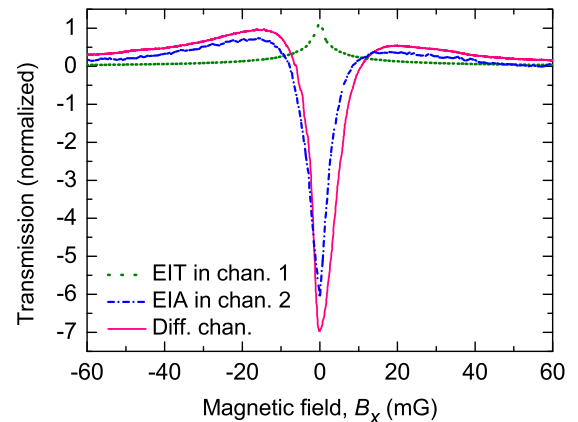

FIG. 10. Level-crossing resonances observed in different channels of the balanced photodetector at $\epsilon = 37°$, $P_t = 1.1\,\mathrm{mW}$, and $T = 60\,°\mathrm{C}$.
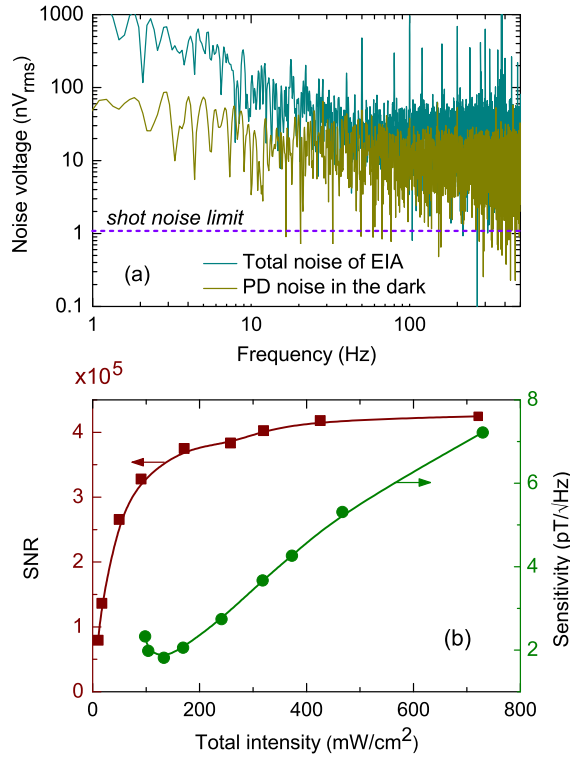
FIG. 11. (a) Noise voltage of the EIA resonance (upper dark cyan curve) at $P_t = 1$ mW and the dark noise of the PD (lower dark yellow curve). (b) SNR (dark red squares along the left y axis) and sensitivity (green circles along the right y axis) at 40 Hz as the work frequency of the sensor versus total intensity of the beam. The conditions for the measurements are $\epsilon = 37°$ and $T = 60°C$.

40 Hz. It has been checked in our experiments (not shown here) that the EIA resonance characteristics do not degrade visibly up to 150 Hz of the scanning frequency. Therefore, we can take a work frequency of the sensor in the range 40–150 Hz. Then, using the dependence of the linewidth in Fig. 7(a), we can now plot the sensitivity δB versus the light-field intensity [Fig. 11(b)]. It reaches approximately 1.8 pT/$\sqrt{\text{Hz}}$ at $I_t \approx 50$ mW/cm^2. This sensitivity is determined mainly by the laser intensity noise, dark noise of the PD, and electric current noise in the Helmholtz coils which is transferred to the intensity noise at the resonance slope. As an example, we show the dark noise of the PD in the same plot. A shot-noise limit shown in the figure as a dashed line is much lower than the observed total noise. Therefore, if all necessary steps are taken to reduce the noise sources, we can expect to achieve a shot-noise-limited sensitivity of approximately 60 fT/$\sqrt{\text{Hz}}$. Some improvement likely can be obtained just by using a differential channel of the PD. However, we do not focus on this possibility in the present study because it deserves separate and careful investigation.

IV. CONCLUSION

In this paper we have considered subnatural-width zero-field level-crossing resonances in a cesium vapor cell with a buffer gas. The effect is also known as the ground-state Hanle effect. The atoms are excited by a single light wave, while a transverse magnetic field is slowly scanned around zero to observe the LCR in the light beam transmission. The buffer-gas pressure is such that the excited-state hyperfine levels of the Cs D_1 line are overlapped due to collisional broadening, while the ground-state hyperfine levels are spectroscopically resolved. Based on a three-level Λ scheme, we developed a simplified theory that provides an explicit analytical solution for the light-wave absorption index. The solution revealed a line-narrowing effect that can be observed in an open system of energy levels. This effect was confirmed experimentally.

The main goal of the paper consisted in developing a single-beam technique that could provide high-quality LCRs in a low-temperature small vapor cell. Such a technique could be of interest in biomedical applications where an array of magnetic-field sensors are required. We have proposed to use a single elliptically polarized light wave that, under the conditions considered, can be treated as a combination of two independent circularly polarized waves: The pump wave creates a strong circular dichroism in the resonant medium, while the probe wave interacts with the prepared atoms. It has been shown that LCRs in the probe-wave transmission demonstrate an extraordinary contrast up to 83% versus 17% as in the standard Hanle scheme. The observed contrast-to-width ratio, a figure of merit of the resonance, reached 42%/mG. It should be emphasized that the observed high characteristics of the resonances have been obtained in a small $5 \times 5 \times 5$ mm^3 vapor cell heated to a relatively low temperature of approximately 60 °C, in contrast to many other schemes where alkali-metal vapors are usually heated to a higher temperature than 120 °C to reach the SERF regime of operation. The absence of the SERF regime in our case also means a potentially large dynamic range of measurements of the sensor up to several microtesla.

The proposed technique for observing the LCRs can be used for developing a high-sensitivity compact magnetic-field sensor of low power consumption and heat release. To demonstrate this, we have measured the noise voltage observed on the photodetector. The noise level appeared to be significantly higher than the shot-noise limit; nevertheless, the estimated sensitivity reached approximately 1.8 pT/$\sqrt{\text{Hz}}$ at 40 Hz. We expect that additional efforts directed at the noise suppression will help us demonstrate the shot-noise-limited sensitivity of approximately 60 fT/$\sqrt{\text{Hz}}$. However, such a systematic work deserves a separate study.

In our experiments, a pair of Helmholtz coils is used to scan the transverse field B_x to observe the resonance. The resonance shift provides information about the x component of the ambient magnetic field that can be measured. A two-dimensional operation of the sensor can be easily realized by using the second pair of coils to scan B_y field. A full three-dimensional (vector) mode of operation can be also realized in different ways. One of them is to use additional coils to compensate for the z component of the ambient field by maximization of the resonance contrast. Another way is to monitor the resonance linewidth that experiences additional linear broadening if B_z is presented in the cell [35]. Also, all three components of the field can be measured by scanning the transverse and longitudinal magnetic fields to observe different types of LCRs [73].

Finally, we would like to point out that the small vapor cell used in our experiments can be integrated into a compact magnetic-field sensor, as has already been demonstrated by other groups with similar cubic glass vapor cells (see, e.g., [39,92]). However, what is truly breathtaking is the possibility of using the proposed technique in conjunction with the booming photonic-atomic chip-scale technologies that provide extreme miniaturization. For instance, a photon spin sorter was recently demonstrated in [93]. Such a device is probably best suited for creating a chip-scale circular-dichroism-based quantum sensor.

APPENDIX

Here we apply a well-known density matrix approach [67] to figure out analytical expressions for absorption indices of the pump and probe waves in atomic vapors. We start from the general equation (2), where the free-atom Hamiltonian has the explicit form

$$\hat{H}_0 = \sum_{n=0}^{3} \mathcal{E}_n |n\rangle\langle n|, \tag{A1}$$

where $\mathcal{E}_n$ is an energy of n level with $\mathcal{E}_1 = \mathcal{E}_2$ [see Fig. 1(b)] so that $\omega_{31} = \omega_{32} = (\mathcal{E}_3 - \mathcal{E}_1)/\hbar$ is the optical transition frequencies in the Λ scheme. Angular brackets $\langle \cdots |$ and $| \cdots \rangle$ stand for the Dirac's bra and ket vectors, respectively.

The operator $\hat{V}_b$ is responsible for the interaction between the atomic spins and ambient transverse magnetic field ($\mathbf{B}_x \perp \mathbf{k}$). It leads to mixing of the $|1\rangle$ and $|2\rangle$ states

$$\hat{V}_b = \hbar\Omega(|1\rangle\langle 2| + |2\rangle\langle 1|), \tag{A2}$$

where Ω is the Larmor frequency.

In the rotating-wave approximation, the interaction between the atomic dipole momentum d and the light field (1) is described by the operator

$$\hat{V}_e = -\hat{d}E(t,z) = -\hbar R_c e^{-i\omega t}|3\rangle\langle 1|$$
$$- \hbar R_p e^{-i\omega t}|3\rangle\langle 2| + \text{H.c.}, \tag{A3}$$

with $R_{c,p}$ the Rabi frequencies for the pump (c) and probe (p) waves and H.c. the Hermitian conjugate terms. As shown in Sec. II, the pump wave experiences low absorption in the cell. The probe wave in turn is weak enough to not affect the atomic density matrix at all. Therefore, we do not take into account the dependence of the Rabi frequencies on the z coordinate in (A3).

The density matrix $\hat{\rho}$ for the Λ scheme considered can be written in the form

$$\hat{\rho} = \begin{pmatrix} \rho_{00} & 0 & 0 & 0 \\ 0 & \rho_{11} & \rho_{12} & \rho_{13} \\ 0 & \rho_{21} & \rho_{22} & \rho_{23} \\ 0 & \rho_{31} & \rho_{32} & \rho_{33} \end{pmatrix}, \tag{A4}$$

where diagonal elements ρ_{nn} ($n = 0, \ldots, 3$) denote the sublevel populations, ρ_{12} and ρ_{21} stand for the so-called Zeeman coherences, and ρ_{13}, ρ_{31}, ρ_{23}, and ρ_{32} are known as optical coherences because they oscillate in time at the optical frequency ω. Other nondiagonal elements, such as ρ_{0n} and ρ_{n0} ($n = 1, \ldots, 3$), are equal to zero because there is no light or microwave field in the system that could couple the corresponding sublevels. Therefore, $|0\rangle$ can be referred to as the trap state with the population ρ_{00}. Since the density matrix is Hermitian, $\hat{\rho} = \hat{\rho}^\dagger$, we get the relation $\rho_{nm} = \rho_{mn}^*$.

The relaxation operator $\hat{\mathcal{R}}$ in (2) reflects the influence of three different processes in the atom: spontaneous radiation emission from the excited state occurring at the rate 2γ, collisional broadening of the optical absorption line (γ_c), and diffusive motion of alkali-metal atoms in buffer gas (Γ), during which a spin-polarized atom either leaves the light beam or undergoes a spin-exchange–destruction collision (see review [88]). We can consider these contributions by separate terms, namely, the spontaneous relaxation reads

$$\hat{\mathcal{R}}_{\text{spon}} = \gamma \begin{pmatrix} \beta_0\rho_{33} & 0 & 0 & -1 \\ 0 & \beta_1\rho_{33} & 0 & -1 \\ 0 & 0 & \beta_2\rho_{33} & -1 \\ -1 & -1 & -1 & -2 \end{pmatrix}, \tag{A5}$$

where the branching ratios are $\beta_1 = \beta_2 \equiv \beta$ and $\beta_0 = 2(1 - \beta)$. The collisional line broadening is described by the terms

$$\hat{\mathcal{R}}_{\text{coll}} = -\gamma_c \sum_{n=1}^{2} \rho_{n3}|n\rangle\langle 3| + \text{H.c.}, \tag{A6}$$

Finally, the diffusion time-of-flight relaxation has the form

$$\hat{\mathcal{R}}_{\text{diff}} = -\Gamma\hat{\rho} + \frac{1}{3}\Gamma \sum_{n=0}^{2} |n\rangle\langle n|. \tag{A7}$$

Here we take into account that the initial (isotropic) population distribution is such that $\rho_{00} = \rho_{11} = \rho_{22} = \frac{1}{3}$.

We apply the rotating-wave approximation, which means the following series expansion for the optical coherences:

$$\rho_{13}(t) = \tilde{\rho}_{13}e^{i\omega t}, \quad \rho_{23}(t) = \tilde{\rho}_{23}e^{i\omega t},$$
$$\rho_{31}(t) = \tilde{\rho}_{31}e^{-i\omega t}, \quad \rho_{32}(t) = \tilde{\rho}_{32}e^{-i\omega t}. \tag{A8}$$

We consider the atom-field interaction under the optical resonance condition when $\omega = \omega_{31} = \omega_{32}$. Using the master equation (2) and all the above expressions, we arrive at the set of linear differential equations

$$\frac{d}{dt}\rho_{00} = \frac{1}{3}\Gamma + 2(1-\beta)\gamma\rho_{33} - \Gamma\rho_{00}, \tag{A9}$$

$$\frac{d}{dt}\rho_{11} = \frac{1}{3}\Gamma + \beta\gamma\rho_{33} - \Gamma\rho_{11}$$
$$+ i\Omega(\rho_{12} - \rho_{21}) + iR_c(\tilde{\rho}_{31} - \tilde{\rho}_{13}), \tag{A10}$$

$$\frac{d}{dt}\rho_{22} = \frac{1}{3}\Gamma + \beta\gamma\rho_{33} - \Gamma\rho_{22}$$
$$+ i\Omega(\rho_{21} - \rho_{12}) + iR_p(\tilde{\rho}_{32} - \tilde{\rho}_{23}), \tag{A11}$$

$$\frac{d}{dt}\rho_{33} = -2\gamma\rho_{33} - \Gamma\rho_{33} + iR_c(\tilde{\rho}_{13} - \tilde{\rho}_{31})$$
$$+ iR_p(\tilde{\rho}_{23} - \tilde{\rho}_{32}), \tag{A12}$$

$$\frac{d}{dt}\rho_{12} = -\Gamma\rho_{12} + i\Omega(\rho_{11} - \rho_{22})$$
$$+ iR_c\tilde{\rho}_{32} - iR_p\tilde{\rho}_{13}, \tag{A13}$$

$$\frac{d}{dt}\tilde{\rho}_{13} = -\gamma_{eg}\tilde{\rho}_{13} - i\Omega\tilde{\rho}_{23}$$
$$+ iR_c(\rho_{33} - \rho_{11}) - iR_p\rho_{12}, \tag{A14}$$

$$\frac{d}{dt}\tilde{\rho}_{23} = -\gamma_{eg}\tilde{\rho}_{23} - i\Omega\tilde{\rho}_{13}$$
$$+ iR_p(\rho_{33} - \rho_{22}) - iR_c\rho_{21}. \tag{A15}$$

The three other equations for $\tilde{\rho}_{31}$, $\tilde{\rho}_{32}$, and $\tilde{\rho}_{21}$ can be obtained by complex conjugation of the corresponding equations.

The pump wave propagates through the medium according to the reduced wave equation

$$\frac{dE_c}{dz} = 2\pi i k \tilde{P}_c, \tag{A16}$$

where $P_c(z,t) = \tilde{P}_c(z)e^{-i\omega t}$ is the medium polarization induced by the pump wave with $\tilde{P}_c = n_a d_0 \tilde{\rho}_{31}$. Taking into account the relation $I_{p,c} = (c/2\pi)E_{p,c}^2$, we get the equation for the pump-wave intensity change

$$\frac{dI_c}{dz} = 2n_a\hbar\omega R_c \text{Im}(\tilde{\rho}_{13}). \tag{A17}$$

Considering the steady-state regime, when the complex amplitudes $\tilde{\rho}_{nm}$ in (A8) do not depend on time as well as the sublevel populations ρ_{nn} and Zeeman coherences ρ_{12} and ρ_{21}, we arrive at the expression

$$\tilde{\rho}_{13} = \frac{i\gamma_{eg}R_c}{\Omega^2 + \gamma_{eg}^2}(\rho_{33} - \rho_{11}) - \frac{R_c\Omega}{\Omega^2 + \gamma_{eg}^2}\rho_{21}$$
$$+ \frac{R_p\Omega}{\Omega^2 + \gamma_{eg}^2}(\rho_{33} - \rho_{22}) - \frac{i\gamma_{eg}R_p}{\Omega^2 + \gamma_{eg}^2}\rho_{12}. \tag{A18}$$

In a linear approximation on the probe field, we can take $R_p = 0$ in the formula (A18). We also assume that $\Omega \ll \gamma_{eg}$ and $R_c \ll \gamma_{eg}$, so (A18) now reads

$$\tilde{\rho}_{13} \approx i\frac{R_c}{\gamma_{eg}}(\rho_{33} - \rho_{11}). \tag{A19}$$

This expression means that the optical coherence on the transition $|1\rangle \rightarrow |3\rangle$ is created by the pump light field rather than the interference action of the probe light field and the transverse magnetic field. In our approach, this coherence contains only the imaginary part, i.e., any effects of birefringence, such as the Voigt (Cotton-Mouton) effect [10], are negligible in comparison to dichroism effects under the optical resonance condition $\omega = \omega_{32} = \omega_{31}$ considered in the present work.

By substituting (A19) into (A12) and taking $R_p = 0$, in the steady state we get

$$\rho_{33} \approx \frac{2R_c^2\tau}{\gamma_{eg}(1 + 2\gamma\tau)}(\rho_{11} - \rho_{33}). \tag{A20}$$

In this equation we can assume $\gamma\tau \gg 1$, which is satisfied with a good margin in the case of a buffered vapor cell. Furthermore, due to a large collisional broadening of the optical absorption line, we also have the condition $R_c^2 \ll \gamma\gamma_{eg}$. These assumptions lead to a simple solution

$$\rho_{33} \approx \frac{R_c^2}{\gamma\gamma_{eg}}\rho_{11}, \tag{A21}$$

meaning that $\rho_{33} \ll \rho_{11}$. Therefore, we can neglect the influence of the excited-state population on the pump-wave absorption in the cell. All these conclusions result in the law

$$\frac{dI_c}{dz} \approx -\frac{2n_a\hbar\omega}{\gamma_{eg}}\rho_{11}R_c^2 = -\frac{3\gamma\beta\lambda^2 n_a}{4\pi\gamma_{eg}}\rho_{11}I_c, \tag{A22}$$

which coincides with (3).

To find the steady-state population ρ_{11}, we assume that the Zeeman coherences ρ_{12} and ρ_{21} are produced only by the magnetic field. This assumption is valid because, as mentioned at the beginning of Sec. II, the interference between the pump and the probe waves can be neglected. If $R_c \ll \gamma_{eg}$ and $\Omega \ll \gamma_{eg}$, then we find

$$\rho_{12} \approx \frac{i\Omega\tau}{1 + \xi}(\rho_{11} - \rho_{22}), \tag{A23}$$

with $\rho_{21} = \rho_{12}^*$.

Substituting (A19) and (A23) into (A10) and assuming $\rho_{33} \ll \rho_{11}$, we arrive at the solution

$$\rho_{11} \approx \rho_0 \frac{1 + \xi + 4\Omega^2\tau^2}{(1 + \xi)\chi + 4\Omega^2\tau^2(\chi - \xi)}, \tag{A24}$$

with $\chi = 1 + (2 - \beta)\xi$. In combination with (A22), the expression (A24) results in the pump-wave absorption index (7). In (A24), $\rho_0 = \frac{1}{3}$ is the initial sublevel population in the absence of the light field.

Similarly to (A17), the probe-wave absorption satisfies the equation

$$\frac{dI_p}{dz} = 2n_a\hbar\omega R_p \text{Im}(\tilde{\rho}_{23}). \tag{A25}$$

At $\Omega \ll \gamma_{eg}$, from (A15) we get

$$\tilde{\rho}_{23} \approx i\frac{R_p}{\gamma_{eg}}(\rho_{33} - \rho_{22}) + i\frac{R_c}{\gamma_{eg}}\rho_{12}, \tag{A26}$$

and (A25) now transforms to

$$\frac{dI_p}{dz} = \frac{2n_a\hbar\omega}{\gamma_{eg}}\big[R_p^2(\rho_{33} - \rho_{22}) - R_pR_c\text{Re}(\rho_{12})\big]. \tag{A27}$$

Neglecting the low impact from the excited-state population and the influence of the interference term (proportional to R_cR_p) gives

$$\frac{dI_p}{dz} \approx -\frac{2n_a\hbar\omega}{\gamma_{eg}}\rho_{22}R_p^2 = -\frac{3\gamma\beta\lambda^2 n_a}{4\pi\gamma_{eg}}\rho_{22}I_p, \tag{A28}$$

where ρ_{22} does not depend on the probe field in the linear regime. In addition, since the pump field experiences low absorption in the cell (discussed in the main text), ρ_{22} does not

depend on z as well. Therefore, we can easily get an explicit solution in the form

$$I_p(z) = I_{p0}e^{-\alpha_p z}, \qquad (A29)$$

with I_{p0} the probe-wave intensity at the entrance of the cell and α_p the probe-wave absorption index

$$\alpha_p \approx \frac{3\gamma\beta\lambda^2 n_a}{4\pi\gamma_{eg}}\rho_{22}. \qquad (A30)$$

Using the same assumptions ($R_c^2 \ll \gamma\gamma_{eg}$ and $\Omega \ll \gamma_{eg}$), the steady-state solution of (A11) gives

$$\rho_{22} \approx \rho_0 \frac{(1+\xi)(1+2\xi)+4\Omega^2\tau^2}{(1+\xi)\chi+4\Omega^2\tau^2(\chi-\xi)}, \qquad (A31)$$

which results in the probe-wave absorption index (12).

[1] I. K. Kominis, T. W. Kornack, J. C. Allred, and M. V. Romalis, Nature (London) **422**, 596 (2003).

[2] O. Alem, T. H. Sander, R. Mhaskar, J. LeBlanc, H. Eswaran, U. Steinhoff, Y. Okada, J. Kitching, L. Trahms, and S. Knappe, Phys. Med. Biol. **60**, 4797 (2015).

[3] E. J. Pratt *et al.*, in *Optical and Quantum Sensing and Precision Metrology*, edited by S. M. Shahriar and J. Scheuer, SPIE Proc. Vol. 11700 (SPIE, Bellingham, 2021), p. 1170032.

[4] J. Marquetand, T. Middelmann, J. Dax, S. Baek, D. Sometti, A. Grimm, H. Lerche, P. Martin, C. Kronlage, M. Siegel, C. Braun, and P. Broser, Clin. Neurophysiol. **132**, 2681 (2021).

[5] A. Soheilian, M. M. Tehranchi, and M. Ranjbaran, Sci. Rep. **11**, 7156 (2021).

[6] A. Fabricant, G. Z. Iwata, S. Scherzer, L. Bougas, K. Rolfs, A. Jodko-Władzińska, J. Voigt, R. Hedrich, and D. Budker, Sci. Rep. **11**, 1438 (2021).

[7] P. Put, S. Pustelny, D. Budker, E. Druga, T. F. Sjolander, A. Pines, and D. A. Barskiy, Anal. Chem. **93**, 3226 (2021).

[8] G. Breit, Rev. Mod. Phys. **5**, 91 (1933).

[9] W. Gawlik, D. Gawlik, and H. Walther, in *The Hanle Effect and Level-Crossing Spectroscopy*, edited by G. Moruzzi and F. Strumia (Springer, New York, 1991), p. 47.

[10] D. Budker, W. Gawlik, D. F. Kimball, S. M. Rochester, V. V. Yashchuk, and A. Weis, Rev. Mod. Phys. **74**, 1153 (2002).

[11] W. Hanle, Z. Phys. **30**, 93 (1924).

[12] E. B. Aleksandrov, A. M. Bonch-Bruevich, and V. A. Khodovoi, Opt. Spectrosc. **23**, 151 (1967).

[13] J. Dupont-Roc, S. Haroche, and C. Cohen-Tannoudji, Phys. Lett. **28A**, 638 (1969).

[14] J. C. Lehmann and C. Cohen-Tannoudji, C. R. Acad. Sci. (Paris) **258**, 4463 (1964).

[15] A. L. Bloom, Appl. Opt. **1**, 61 (1962).

[16] E. B. Alexandrov and A. K. Vershovskiy, in *Optical Magnetometry*, edited by D. Budker and D. F. Jackson Kimball (Cambridge University Press, Cambridge, 2013), p. 60.

[17] V. Shah, S. Knappe, P. D. D. Schwindt, and J. Kitching, Nat. Photon. **1**, 649 (2007).

[18] R. Mhaskar, S. Knappe, and J. Kitching, Appl. Phys. Lett. **101**, 241105 (2012).

[19] J.-J. Li, P.-C. Du, J.-Q. Fu, X.-T. Wang, Q. Zhou, and R.-Q. Wang, Chin. Phys. B **28**, 040703 (2019).

[20] J. C. Allred, R. N. Lyman, T. W. Kornack, and M. V. Romalis, Phys. Rev. Lett. **89**, 130801 (2002).

[21] R. Jiménez-Martínez, W. C. Griffith, Y. Wang, S. Knappe, J. Kitching, K. Smith, and M. D. Prouty, IEEE Trans. Instrum. Meas. **59**, 372 (2010).

[22] C. Andreeva, S. Cartaleva, Y. Dancheva, V. Biancalana, A. Burchianti, C. Marinelli, E. Mariotti, L. Moi, and K. Nasyrov, Phys. Rev. A **66**, 012502 (2002).

[23] A. V. Papoyan, M. Auzinsh, and K. Bergmann, Eur. Phys. J. D **21**, 63 (2002).

[24] M. Auzinsh, R. Ferber, F. Gahbauer, A. Jarmola, and L. Kalvans, Phys. Rev. A **78**, 013417 (2008).

[25] S. Gozzini, S. Cartaleva, A. Lucchesini, C. Marinelli, L. Marmugi, D. Slavov, and T. Karaulanov, Eur. Phys. J. D **53**, 153 (2009).

[26] L. Marmugi, S. Gozzini, A. Lucchesini, A. Bogi, A. Burchianti, and C. Marinelli, J. Opt. Soc. Am. B **29**, 2729 (2012).

[27] H. Ravi, M. Bhattarai, V. Bharti, and V. Natarajan, Europhys. Lett. **117**, 63002 (2017).

[28] V. G. Lucivero, P. Anielski, W. Gawlik, and M. W. Mitchell, Rev. Sci. Instrum. **85**, 113108 (2014).

[29] N. Wilson, P. Light, A. Luiten, and C. Perrella, Phys. Rev. Applied **11**, 044034 (2019).

[30] M. Klein, M. Hohensee, D. F. Phillips, and R. L. Walsworth, Phys. Rev. A **83**, 013826 (2011).

[31] S. Gozzini, A. Fioretti, A. Lucchesini, L. Marmugi, C. Marinelli, S. Tsvetkov, S. Gateva, and S. Cartaleva, Opt. Lett. **42**, 2930 (2017).

[32] D. V. Brazhnikov, S. M. Ignatovich, V. I. Vishnyakov, M. N. Skvortsov, C. Andreeva, V. M. Entin, and I. I. Ryabtsev, Laser Phys. Lett. **15**, 025701 (2018).

[33] G. Le Gal, G. Lieb, F. Beato, T. Jager, H. Gilles, and A. Palacios-Laloy, Phys. Rev. Applied **12**, 064010 (2019).

[34] D. V. Brazhnikov, S. M. Ignatovich, A. S. Novokreshchenov, and M. N. Skvortsov, J. Phys. B **52**, 215002 (2019).

[35] D. V. Brazhnikov, V. I. Vishnyakov, S. M. Ignatovich, I. S. Mesenzova, C. Andreeva, and A. N. Goncharov, Appl. Phys. Lett. **119**, 024001 (2021).

[36] E. Breschi, Z. D. Grujić, P. Knowles, and A. Weis, Appl. Phys. Lett. **104**, 023501 (2014).

[37] S. N. Nikolić, M. Radonjić, N. M. Lučić, A. J. Krmpot, and B. M. Jelenković, Phys. Scr. **T162**, 014038 (2014).

[38] L. Lenci, L. Marmugi, F. Renzoni, S. Gozzini, A. Lucchesini, and A. Fioretti, J. Phys. B **52**, 085002 (2019).

[39] V. Shah and M. V. Romalis, Phys. Rev. A **80**, 013416 (2009).

[40] J. Tang, Y. Zhai, L. Cao, Y. Zhang, L. Li, B. Zhao, B. Zhou, B. Han, and G. Liu, Opt. Express **29**, 15641 (2021).

[41] A. Ben-Kish and M. V. Romalis, Phys. Rev. Lett. **105**, 193601 (2010).

[42] M. V. Petrenko, A. S. Pazgalev, and A. K. Vershovskii, Phys. Rev. Applied **15**, 064072 (2021).

[43] Y. Ma, J. Deng, Z. Hu, H. He, and Y. Wang, Chin. Opt. Lett. **11**, 022701 (2013).

[44] S. Pradhan and R. Behera, Sensor Actuat. A **290**, 48 (2019).

[45] A. Papoyan, S. Shmavonyan, A. Khanbekyan, K. Khanbekyan, C. Marinelli, and E. Mariotti, Appl. Opt. **55**, 892 (2016).

[46] D. Brazhnikov, S. Ignatovich, I. Mesenzova, A. Novokreshchenov, and A. Goncharov, Opt. Lett. **45**, 3309 (2020).

[47] E. Pfleghaar, J. Wurster, S. I. Kanorsky, and A. Weis, Opt. Commun. **99**, 303 (1993).

[48] Y. Dancheva, G. Alzetta, S. Cartaleva, M. Taslakov, and C. Andreeva, Opt. Commun. **178**, 103 (2000).

[49] K.-J. Boller, A. Imamoğlu, and S. E. Harris, Phys. Rev. Lett. **66**, 2593 (1991).

[50] A. M. Akulshin, S. Barreiro, and A. Lezama, Phys. Rev. A **57**, 2996 (1998).

[51] J. Dimitrijević, A. Krmpot, M. Mijailović, D. Arsenović, B. Panić, Z. Grujić, and B. M. Jelenković, Phys. Rev. A **77**, 013814 (2008).

[52] Y. J. Yu, H. J. Lee, I.-H. Bae, H.-R. Noh, and H. S. Moon, Phys. Rev. A **81**, 023416 (2010).

[53] H.-R. Noh and H. S. Moon, Phys. Rev. A **82**, 033407 (2010).

[54] R. S. Grewal and M. Pattabiraman, J. Phys. B **48**, 085501 (2015).

[55] D. B. Lazebnyi, D. V. Brazhnikov, A. V. Taichenachev, M. Y. Basalaev, and V. I. Yudin, J. Exp. Theor. Phys. **121**, 934 (2015).

[56] H. Failache, P. Valente, G. Ban, V. Lorent, and A. Lezama, Phys. Rev. A **67**, 043810 (2003).

[57] D. V. Brazhnikov, A. V. Taichenachev, A. M. Tumaikin, and V. I. Yudin, J. Opt. Soc. Am. B **22**, 57 (2005).

[58] J. Belfi, V. Biancalana, S. Cartaleva, Y. Dancheva, E. Mariotti, L. Moi, K. Nasyrov, D. Slavov, P. Todorov, and K. Vaseva, Acta Phys. Pol. A **112**, 823 (2007).

[59] Z. A. S. Jadoon, H. R. Noh, and J. T. Kim, Sci. Rep. **12**, 145 (2022).

[60] E. Arimondo and G. Orriols, Lett. Nuovo Cimento **17**, 333 (1976).

[61] D. A. Varshalovich, A. N. Moskalev, and V. K. Khersonskii, *Quantum Theory of Angular Momentum* (World Scientific, Singapore, 1988).

[62] E. Arimondo, Prog. Opt. **35**, 257 (1996).

[63] L. Margalit, M. Rosenbluh, and A. D. Wilson-Gordon, Phys. Rev. A **87**, 033808 (2013).

[64] D. V. Brazhnikov, G. Coget, M. A. Hafiz, V. Maurice, C. Gorecki, and R. Boudot, IEEE Trans. Ultrason. Ferroelectr. Freq. Control **65**, 962 (2018).

[65] D. V. Brazhnikov, A. V. Taichenachev, A. M. Tumaikin, and V. I. Yudin, Laser Phys. Lett. **11**, 125702 (2014).

[66] D. Brazhnikov, S. Ignatovich, V. Vishnyakov, R. Boudot, and M. Skvortsov, Opt. Express **27**, 36034 (2019).

[67] K. Blum, *Density Matrix Theory and Applications* (Springer, Berlin, 2012).

[68] E. Alipieva, S. Gateva, and E. Taskova, in *Proceedings of the Eighth International Conference on Laser and Laser Information Technologies, Smolyan, 2003*, edited by V. Y. Panchenko and N. V. Sabotinov, SPIE Proc. Vol. 5449 (SPIE, Bellingham, 2004), p. 336.

[69] H.-b. Zhang, G. Yang, G.-m. Huang, and G.-x. Li, Phys. Rev. A **99**, 033803 (2019).

[70] C. Cohen-Tannoudji, J. Dupont-Roc, S. Haroche, and F. Laloë, Rev. Phys. Appl. **5**, 95 (1970).

[71] J. Vanier, A. Godone, and F. Levi, Phys. Rev. A **58**, 2345 (1998).

[72] H. Lee, Y. Rostovtsev, C. J. Bednar, and A. Javan, Appl. Phys. B **76**, 33 (2003).

[73] G. Le Gal and A. Palacios-Laloy, Phys. Rev. A **105**, 052213 (2022).

[74] J. W. Pollock, V. I. Yudin, A. V. Taichenachev, M. Y. Basalaev, D. V. Kovalenko, A. Hansen, J. Kitching, and W. R. McGehee, Appl. Phys. Lett. **120**, 154001 (2022).

[75] S. A. Zibrov, Y. O. Dudin, A. G. Radnaev, V. V. Vassiliev, V. L. Velichansky, D. V. Brazhnikov, A. V. Taāchenachev, and V. I. Yudin, JETP Lett. **85**, 417 (2007).

[76] D. V. Brazhnikov, A. V. Taichenachev, A. M. Tumaikin, V. I. Yudin, I. I. Ryabtsev, and V. M. Entin, JETP Lett. **91**, 625 (2010).

[77] I. S. Radojiāić, M. Radonjić, M. M. Lekić, Z. D. Grujić, D. Lukić, and B. Jelenković, J. Opt. Soc. Am. B **32**, 426 (2015).

[78] D. A. Steck, Cesium D line data, https://steck.us/alkalidata/cesiumnumbers.pdf

[79] F. Renzoni, W. Maichen, L. Windholz, and E. Arimondo, Phys. Rev. A **55**, 3710 (1997).

[80] A. S. Zibrov and A. B. Matsko, JETP Lett. **82**, 472 (2005).

[81] M. Auzinsh, A. Berzins, R. Ferber, F. Gahbauer, L. Kalvans, A. Mozers, and D. Opalevs, Phys. Rev. A **85**, 033418 (2012).

[82] H.-J. Kang and H.-R. Noh, Opt. Express **25**, 21762 (2017).

[83] A. V. Taichenachev, A. M. Tumaikin, and V. I. Yudin, JETP Lett. **72**, 119 (2000).

[84] A. Javan, O. Kocharovskaya, H. Lee, and M. O. Scully, Phys. Rev. A **66**, 013805 (2002).

[85] S. Appelt, A. B. Baranga, A. R. Young, and W. Happer, Phys. Rev. A **59**, 2078 (1999).

[86] F. Levi, A. Godone, J. Vanier, S. Micalizio, and G. Modugno, Eur. Phys. J. D **12**, 53 (2000).

[87] A. V. Taichenachev, A. M. Tumaikin, V. I. Yudin, M. Stähler, R. Wynands, J. Kitching, and L. Hollberg, Phys. Rev. A **69**, 024501 (2004).

[88] W. Happer, Rev. Mod. Phys. **44**, 169 (1972).

[89] J. Vanier and C. Audoin, *The Quantum Physics of Atomic Frequency Standards* (Hilger, Bristol, 1989).

[90] F. A. Franz and E. Lüscher, Phys. Rev. **135**, A582 (1964).

[91] L. C. Ha, X. Zhang, N. Dao, and K. R. Overstreet, Phys. Rev. A **103**, 022826 (2021).

[92] E. Boto *et al.*, NeuroImage **149**, 404 (2017).

[93] Y. Sebbag, A. Naiman, E. Talker, Y. Barash, and U. Levy, ACS Photon. **8**, 142 (2021).